Journal of Solid State Chemistry 211 (2014) 170–175

Contents lists available at ScienceDirect

Journal of Solid State Chemistry

journal homepage: www.elsevier.com/locate/jssc

Lithium-cation conductivity and crystal structure of lithium diphosphate

V.I. Voronin [a], E.A. Sherstobitova [a], V.A. Blatov [b,c], G.Sh. Shekhtman [d,*]

[a] Institute of Metal Physics Urals Branch RAS, S.Kovalevskoy Street 18, 620041 Ekaterinburg, Russia
[b] Samara Center for Theoretical Materials Science (SCTMS), Samara State University, Ac.Pavlov Street 1, 443011 Samara, Russia
[c] Chemistry Department, Faculty of Science, King Abdulaziz University, Jeddah 21589, Saudi Arabia
[d] Institute of High Temperature Electrochemistry Urals Branch RAS, Akademicheskaya 20, 620990 Ekaterinburg, Russia

ARTICLE INFO

Article history:
Received 8 October 2013
Received in revised form
11 December 2013
Accepted 16 December 2013
Available online 25 December 2013

Keywords:
Neutron diffraction
Lithium diphosphate
Solid electrolytes

ABSTRACT

The electrical conductivity of lithium diphosphate $Li_4P_2O_7$ has been measured and jump-like increasing of ionic conductivity at 913 K has been found. The crystal structure of $Li_4P_2O_7$ has been refined using high temperature neutron diffraction at 300–1050 K. At 913 K low temperature triclinic form of $Li_4P_2O_7$ transforms into high temperature monoclinic one, space group $P2_1/n$, $a=8.8261(4)$ Å, $b=5.2028(4)$ Å, $c=13.3119(2)$ Å, $\beta=104.372(6)^\circ$. The migration maps of Li^+ cations based on experimental data implemented into program package TOPOS have been explored. It was found that lithium cations in both low- and high temperature forms of $Li_4P_2O_7$ migrate in three dimensions. Cross sections of the migrations channels extend as the temperature rises, but at the phase transition point have a sharp growth showing a strong "crystal structure – ion conductivity" correlation.

1. Introduction

Solid electrolytes with lithium ion conductivity are intensively investigated at present because their use in power sources with lithium or lithium alloys anodes holds much promise. A lot of lithium ion conducting materials with a large variety of structural types have been obtained by now [1,2]. In particular, lithium diphosphate $Li_4P_2O_7$ has rather high Li^+ conductivity ($\sim 10^{-1}$ S cm^{-1} at 925 K [3]) which furthermore may be enhanced by heterovalent substitutions [4]. To understand the conductivity mechanism of solid electrolytes the knowledge of their crystal structure peculiarities in the wide temperature range is necessary. Data on crystal structure of $Li_4P_2O_7$ at room temperature have been obtained by X-ray analysis of single crystals are controversial [5,6]. According to [5], the crystal lattice of $Li_4P_2O_7$ is monoclinic, space group $P2_1/n$, $a=5.190(2)$, $b=13.902(3)$, $c=7.901(3)$ Å, $\beta=89.97(3)^\circ$, $z=4$. Another model was proposed later: according to [6], the crystal structure of $Li_4P_2O_7$ at room temperature is interpreted as triclinic, space group P-1, $a=8.5613(4)$, $b=7.1100(3)$, $c=5.18510(10)$ Å, $\alpha=111.44(2)^\circ$, $\beta=89.986(3)^\circ$, $\gamma=103.065(4)^\circ$, $z=2$. This model was confirmed by data of the computer modeling of optimized crystal structures of several lithium phosphates and thiophosphates, in particular, $Li_4P_2O_7$ [7]. The lattice parameters and coordinates of atoms conform rather well to the data [6]. The conclusion on triclinic lattice of low temperature form of $Li_4P_2O_7$ is confirmed by the investigation of the phase relations in the system $ZnO–Li_2O–P_2O_5$ [8] too. Some discrepancy in the values of the structural parameters reported in different papers is probably the result of poor sensitivity of the X-rays to such light elements as lithium and oxygen. A lot of researchers of lithium compounds had to deal with this problem [9–13]. So neutron diffraction is the most preferable method for studying the structural peculiarities of the solid electrolytes containing light atoms.

In [7], the migration energy barrier for lithium vacancies at room temperature for one of the possible paths was evaluated based on the model of the crystal lattice of $Li_4P_2O_7$ using the computer modeling. However, the most detailed analysis of migration paths in solid electrolytes may be carried out using the program package TOPOS [14]. It permits to explore the migration maps based on the experimental structural parameters. This program package was successfully used for exploring migration maps of many solid electrolytes and, in particular, for low temperature form of $KAlO_2$ [15].

It should be mentioned that until now the crystal structure of lithium diphosphate has only been studied at room temperature, while for exploration of ionic conductivity, an investigation of its structure at high temperature is necessary. So the goal of this work was an investigation of the conductivity mechanism of $Li_4P_2O_7$ based on the study of its crystal structure by means of powder neutron diffraction over a wide temperature range as well as on migration maps of Li^+ ions built with the program package TOPOS.

2. Materials and methods

Conventional solid-state reaction procedure was employed to prepare $Li_4P_2O_7$ compound. The starting materials were Li_2CO_3

* Corresponding author. Tel.: +73 433 623 537.
E-mail addresses: voronin@imp.uran.ru (V.I. Voronin), blatov@samsu.ru (V.A. Blatov), shekhtman@ihte.uran.ru (G.Sh. Shekhtman).

0022-4596/$ - see front matter © 2013 Elsevier Inc. All rights reserved.
http://dx.doi.org/10.1016/j.jssc.2013.12.015

(reagent grade) and $NH_4H_2PO_4$ (analytical grade). Appropriate amounts of the starting materials were weighed within the accuracy of $\pm 10^{-4}$ g using an FX-40CJ analytical balance, mixed in a jasper mortar and sintered in an alundum crucible at 500 K for 10–12 h. The resulting mass was reground and heated again. The final temperature was 1070 ± 10 K. The pellets for conductivity measurement were prepared by pressing fine powder in a steel die at ~300 MPa. The pressed pellets were sintered on Pt plate at 1110 ± 10 K. The open porosity of the sintered pellets did not exceed 5%. One pellet was ground for phase characterization employing X-ray powder diffraction (XRD) (Rigaku Dmax-2200, Cu*K*α, Japan) at room temperature. Thermal analysis was performed using STA 449C Jupiter® thermal analyzer (NETZSCH, Germany). Conductivity was measured over the range of 650–1050 K with gold electrodes using P 5083 AC bridge. The frequency range was 100 Hz–100 kHz. The results were plotted as complex impedance plane plots Z'' vs. Z'.

Neutron diffraction experiments were carried out using the high resolution powder neutron diffractometer HRPT (SINQ Spallation source of Paul Scherrer Institute, Villigen, Switzerland) [16]. The sample $Li_4P_2O_7$ was placed in the evacuated vanadium container. Structural parameters were refined by Rietveld technique using Fullprof program [17].

To determine migration maps (i.e. sets of migration paths of mobile cation within the framework) from crystallographic data, we used Voronoi–Dirichlet approach [18] implemented into the program package TOPOS [19].

3. Results and discussion

3.1. Conductivity

According to [20] at 903 K (according to our data at 913 K) the low temperature phase of $Li_4P_2O_7$ transforms into the high temperature one. Over the interval of 720–890 K lithium ion conductivity is 5.6×10^{-3}–3.2×10^{-2} S/cm, activation energy $E = 156 \pm 1$ kJ/mol. With increasing temperature to 920 K conductivity jumps by half an order of magnitude (Fig. 1) and reaches 10^{-1} S/cm, the activation energy decreases down to 80 ± 0.6 kJ/mol. An electronic conductivity over the whole temperature range studied does not exceed 0.1% of total conductivity.

3.2. Crystal structure

3.2.1. Low temperature form (room temperature)

An indexing of the room temperature X-ray pattern of the synthesized sample of $Li_4P_2O_7$ confirms triclinic symmetry (space group *P*-1) proposed in [6]. At a later stage the structural parameters were refined using neutron diffraction data.

Fig. 2 shows the room temperature neutron diffraction pattern of $Li_4P_2O_7$. For preliminary analysis we used the crystallographic data reported in [6]. According to the difference curve, experimental and calculated data are in good agreement. Table 1 lists the crystallographic data and details of the structure refinements of $Li_4P_2O_7$. Using the experimental atom coordinates and lattice parameters we calculated interatomic distances. Data for P and Li are shown in Table 2.

Fig. 3 represents the crystal lattice of $Li_4P_2O_7$. The structure consists of diphosphate groups P_2O_7 arranged by two PO_4 tetrahedra having a common corner. In the PO_4 tetrahedra there is one long P–O distance which corresponds to P–O–P bridge while the other three distances are shorter (Table 2). Li atoms are distributed over 4 unequivalent positions and form distorted tetrahedra LiO_4 (Table 2). Lithium tetrahedra are linked to each other and to P_2O_7 groups by a common vertex or edge and form a continuous framework containing large voids, available for Li^+ ions transport.

Brown's phenomenological Bond Valence Model [21] can help to estimate the correctness of the refined crystal lattice. We calculated valence sums of cations and anions using the experimental bond lengths as $V_i = \Sigma\ (s_{ij})$ where $s_{ij} = \exp\ [(r_o - r_{ij})/B]$, r_o and B are empirical constants determined for each pair of atoms. Table 2 shows that at room temperature the obtained values of V_i are in good agreement with the oxidation state of the ion considered. As empirical constants for bond valence sums calculation are available only at room temperature, calculations at elevated temperatures were not carried out. Some deviation of the valence sums from theoretical values may be the result of the different degree of lithium tetrahedra distortion [22]. The degrees of distortion were calculated as

$$\delta = \sqrt{\sum_{i=1}^{N} \left| 1 - \frac{R_i}{\sum_{i=1}^{N} R_i / N} \right|^2}$$

where R_i is the distance for i pair, $N = 4$ for a tetrahedron. The maximum value of δ is observed for Li_2O_4 tetrahedron, furthermore the average distance Li_2–O (1,99 Å) also exceeds the average distances for other tetrahedra (Table 2). This suggests that the migration of Li^{2+} ions in the low temperature form of $Li_4P_2O_7$ is highly probable. A more detailed description of lithium ions migration will be provided below.

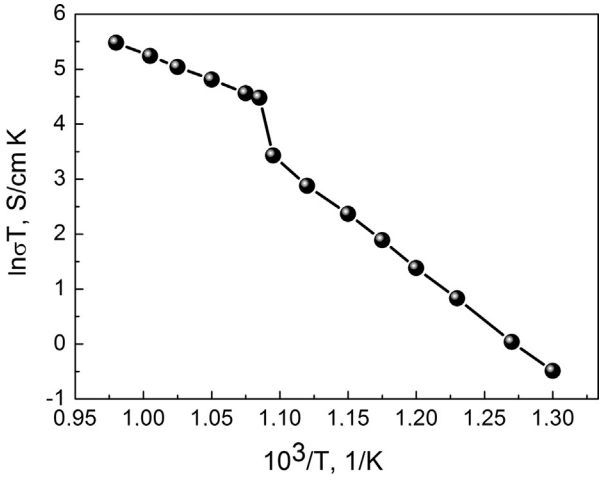

Fig. 1. Temperature dependence of the ionic conductivity for $Li_4P_2O_7$.

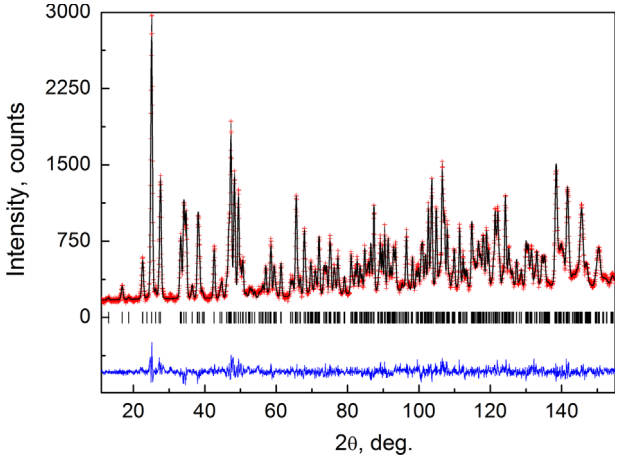

Fig. 2. Fitted powder neutron diffraction profile for $Li_4P_2O_7$ at room temperature. with observed (dots), calculated (solid line) and difference plots. Dashes designate angular positions of reflexes.

Table 1
Crystallographic data for $Li_4P_2O_7$ at different temperatures. Wavelength $\lambda=1.8857$ Å. All atoms sites are fully occupied.

Temperature	$T=300$ K				$T=950$ K			
Crystal system	Triclinic				Monoclinic			
Space group	*P*-1 S.G. (N2)				*P* 1 21/*n* 1 S.G. (N14)			
Lattice constant (Å)	$a=8.5632(6)$, $b=7.1099(7)$, $c=5.1858(4)$, $\alpha=111.426(1)$, $\beta=89.991$ (12), $\gamma=103.055(7)$				$a=8.8264(2)$, $b=5.2024(9)$, $c=13.3106(3)$, $\beta=104.384(2)$			
Volume (Å^3)	285.132(4)				592.05(2)			
Density (g/cm^{-3})	2.349				2.262			
Agreement factors	Bragg *R*-factor=4.37%, $\chi^2=1.955$				Bragg *R*-factor=7.631%, $\chi^2=1.65$			
Atom	*Wyck*	*X*	*Y*	*Z*	*Wyck*	*X*	*Y*	*Z*
P1	2 (*i*)	0.8464(5)	0.2216(7)	0.4380(12)	4 (*e*)	0.1324(10)	0.8421(14)	0.3877(8)
P2	2 (*i*)	0.6316(6)	−0.2150(6)	0.2100(12)	4 (*e*)	0.85352(11)	0.65376(12)	0.10476(4)
O1	2 (*i*)	0.6853(5)	0.0386(6)	0.3097(9)	4 (*e*)	0.9726(16)	0.827(2)	0.0773(12)
O2	2 (*i*)	0.8745(6)	0.2595(8)	0.7428(9)	4 (*e*)	0.8947(19)	0.387(2)	0.1430(12)
O3	2 (*i*)	0.7926(5)	0.3963(7)	0.3883(12)	4 (*e*)	0.7683(19)	0.811(2)	0.1699(13)
O4	2 (*i*)	0.9811(5)	0.1513(6)	0.2723(13)	4 (*e*)	0.720(2)	0.607(2)	0.0087(13)
O5	2 (*i*)	0.6207(7)	−0.2619(8)	0.4748(9)	4 (*e*)	0.4957(17)	0.202(2)	0.0902(13)
O6	2 (*i*)	0.4721(5)	−0.2704(6)	0.0465(12)	4 (*e*)	0.4064(18)	0.588(2)	0.1536(11)
O7	2 (i)	0.7612(6)	−0.2945(7)	0.0411(13)	4 (*e*)	0.259(2)	0.216(2)	0.1658(13)
Li1	2 (*i*)	0.7867(17)	0.6697(19)	0.646 (4)	4 (*e*)	0.728(4)	0.155(7)	0.175(3)
Li2	2 (*i*)	0.4581(19)	0.753(2)	0.695(4)	4 (*e*)	0.027(5)	0.184(7)	0.088(3)
Li3	2 (*i*)	0.7568(16)	0.416(2)	0.017(4)	4 (*e*)	0.179(4)	0.311(7)	0.267(3)
Li4	2 (*i*)	0.7568(16)	0.416(2)	0.017(4)	4 (*e*)	0.509(5)	0.861(6)	0.061(3)

Table 2
Interatomic distances (Å) and bond valence sums of cations for $Li_4P_2O_7$ at room temperature.

Atoms	Distance	Atoms	Distance	Atoms	Distance
P1 – O1	1.612(5)	Li1 – O3	1.92(1)	Li3–O2	1.92(1)
P1–O2	1.511(8)	Li1 – O4	2.07(1)	Li3–O3	1.99(2)
P1 – O3	1.518(8)	Li1 – O5	1.89(2)	Li3–O6	1.97(1)
P1 – O4	1.508(7)	Li1 – O7	2.05(2)	Li3–O7	2.01(1)
P1 – O	**1.538(4)**	**Li1–O**	**1.974(9)**	**Li3–O**	**1.974(9)**
$\delta(\times10^{-4})$	8.0		13.4		3.0
Sum	4.99(5)		1.03(3)		1.02(2)
P2–O1	1.633(6)	Li2–O1	2.14(1)	Li4–O3	1.85(2)
P2–O5	1.516(8)	Li2–O3	2.12(1)	Li4–O4	2.07(1)
P2–O6	1.494(7)	Li2–O5	1.81(1)	Li4–O5	1.99(2)
P–O7	1.498(7)	Li2–O6	1.91(2)	Li4–O7	1.89(1)
P2–O	**1.536(4)**	**Li2–O**	**1.99(1)**	**Li4–O**	**1.950(9)**
$\delta(\times10^{-4})$	13.8		49.5		18.6
Sum	5.04(5)		1.03(3)		1.11(3)

Mean distances are in bold type.

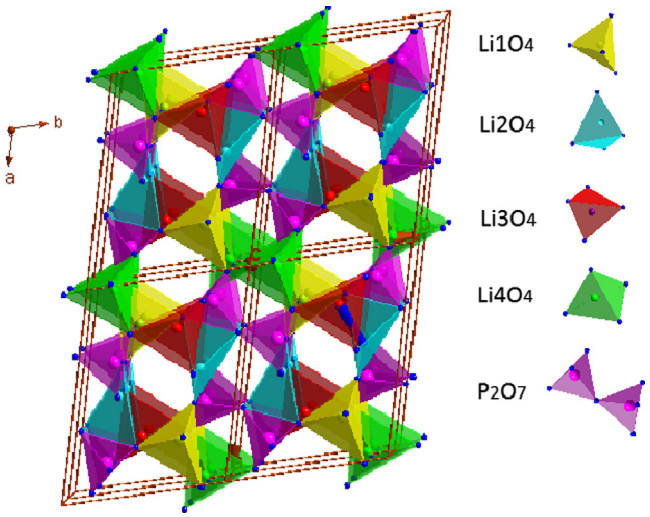

Fig. 3. Structure of $Li_4P_2O_7$ viewed along [001] direction at 300 K.

3.2.2. *Change of crystal structure over 300–900 K*

Between room temperature and 900 K neutron diffraction patterns are similar, so the crystal structure of $Li_4P_2O_7$ corresponds

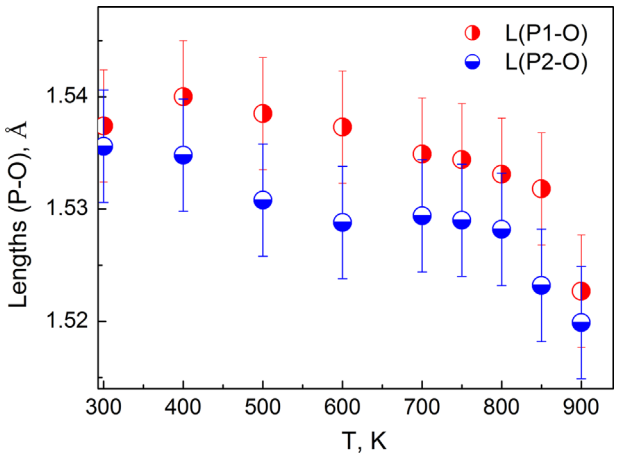

Fig. 4. Temperature dependences of P1–O and P2–O distances in PO_4 tetrahedra of P_2O_7 groups.

to the low temperature form. At the same time, inherent structural peculiarities of the tetrahedral structures appear in the low temperature form of $Li_4P_2O_7$ at heating [15,23–25]. Firstly, the temperature dependence of the $Li_4P_2O_7$ cell parameters indicates a highly anisotropic lattice expansion. The main result of this expansion is that the tetrahedra forming the framework change their orientation. For instance, the turning of PO_4 tetrahedra around the bridge O atoms changes the P–O–P angle of diphosphate groups.

The second peculiarity is an apparent contraction in bond lengths in PO_4 tetrahedra of diphosphate groups with increasing temperature (Fig. 4). Agreement with experimental data for the structures under consideration may be improved by using one of the following three models: (1) the model taking into account the anisotropy of oscillation of the atoms; (2) the so called “split-site” model; (3) the model of the rigid unit mode (RUM). In the case of $Li_4P_2O_7$ using both the first and the second model leaves the P–O distance unaffected. It should be noted, however that there incoherent background in the form of diffuse halos increase in neutron diffraction patterns with rising temperature (Fig. 5). The appearance of these halos may be due to the oscillations of the rigid PO_4 tetrahedra which is consistent with the RUM model. This model is confirmed by data on inelastic neutron scattering: the

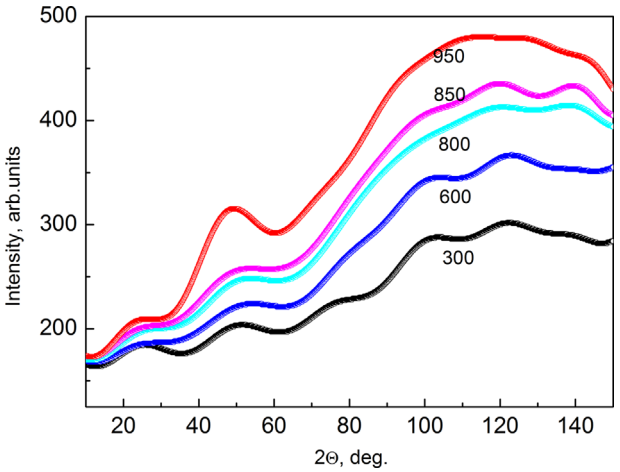

Fig. 5. Angular dependence of the diffuse background intensity for $Li_4P_2O_7$ at different temperatures.

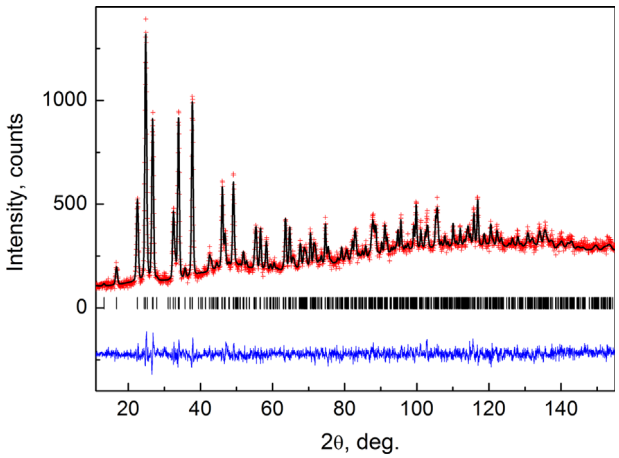

Fig. 7. Fitted powder neutron diffraction profile for $Li_4P_2O_7$ at 1050 K with observed (dots), calculated (solid line) and difference plots. Dashes designate angular positions of reflexes.

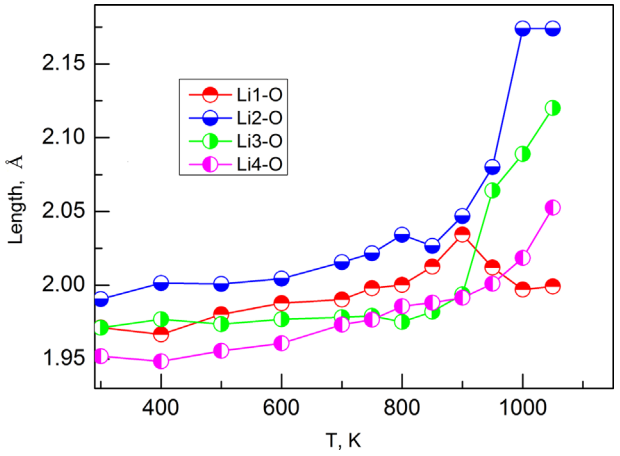

Fig. 6. Temperature dependences of the average Li–O distances for $Li_4P_2O_7$.

spectra obtained for powder SiO_2 samples showed a considerable increase of the low frequency modes with increasing temperature [26]. These results give reason to believe that PO_4 tetrahedra in $Li_4P_2O_7$ are rigid units (RUM model) and to assume the appearance of a dynamic disorder which grows with increasing temperature and consists of a correlation in the movement (oscillation) of the tetrahedra as a whole. In other words, a phenomenon similar to the "paddle-wheel mechanism" [27,28] is registered, which leads to the additional enhancement of ion conductivity. Such a behavior of the background has been observed for many solid electrolytes with Li^+ ion conductivity [29–32].

At the same time, the average Li–O distances show a noticeable increase with increasing temperature (Fig. 6) due to the lattice thermal expansion. The increase of the Li–O distances leads to the bond weakening and to the growth of the Li^+ ions mobility.

3.2.3. *High temperature form of $Li_4P_2O_7$ (950–1050 K)*

Fig. 7 shows the neutron diffraction pattern at 950 K. It can be seen that the neutron diffraction pattern is different from the one at room temperature. According to indexing, the reflections array corresponds to a monoclinic lattice with a doubled cell volume, space group $P12_1/n1$. According to the difference curve, the experimental and calculated data are in good agreement. Table 1 lists the crystallographic data and the details of the structure refinements. To illustrate the relation between triclinic and monoclinic structures we described the triclinic lattice as a distorted pseudo monoclinic one of doubled volume as compared with the triclinic cell. Using this pseudo monoclinic cell we can describe low temperature neutron diffraction patterns. The relation between the parameters of the triclinic and monoclinic cell can be represented in the form [6]: $a_m=a_t$, $b_m=-c_t$, $c_m=2b_t+c_t$. But with the angles different from 90°. Fig. 8 shows temperature dependences of the linear (Fig. 8a) and angular (Fig. 8b) cell parameters. Before phase transition the parameters correspond to the pseudo monoclinic lattice, and after phase transition to the monoclinic one. These dependences confirm the above mentioned conclusion about the anisotropic thermal extension of the $Li_4P_2O_7$ lattice. One can see that α and β angles change most sharply (jump-like) at the phase transition point (Fig. 8b). At the same time, there are no sharp changes in the temperature dependence of the unit cell volume (Fig. 8a, inset).

3.3. *Analysis of migration pattern*

As we saw above, the crystal structure of $Li_4P_2O_7$ is quite complex and it is difficult to analyze the paths of Li^+ ions movement. For this reason, we used the program package TOPOS [14] to explore the migration map. The channel system was calculated using Voronoi–Dirichlet partition of the crystal space according to the procedure described in [18]. The migration maps for $Li_4P_2O_7$ were explored over the whole temperature interval studied (300–1050 K).

Over the 300–900 K interval, we found 26 significant voids (voids suitable for Li^+ ions migration) connected by infinite channels in the triclinic low temperature $Li_4P_2O_7$ form. In the total quantity of the significant voids one can distinguish the voids whose centers coincide with positions of Li1, Li2, Li3 and Li4 atoms. However, we found no significant channel which would connect Li4 position with other significant voids over 300–700 K temperature interval. Therefore, it seems only $Li1^+$, $L2^+$ and $Li3^+$ cations may be charge carriers in $Li_4P_2O_7$ over 300–700 K. The migration of $Li4^+$ ions is unlikely. Over 700–900 K all significant voids and Li1, Li2, Li3 and Li4 positions are connected by significant channels therefore $Li4^+$ ions became potential charge carriers too.

The analysis of the elementary channels with radii exceeding 1.845 Å suitable for Li^+ ions migration [18] as a whole shows that migration map is three-dimensional, nevertheless, it was found that most of the channels are situated in the layers perpendicular

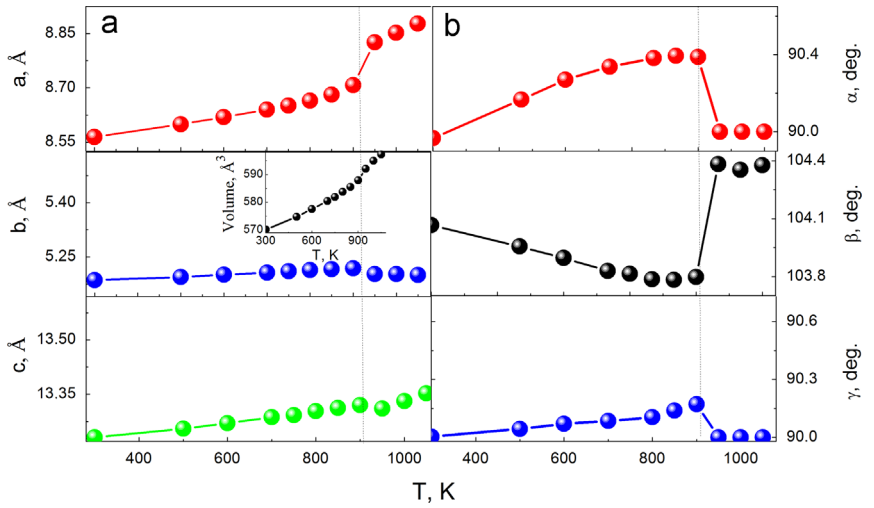

Fig. 8. Temperature dependences of (a) linear, (b) angular parameters and unit cell volume (a, inset) for $Li_4P_2O_7$.

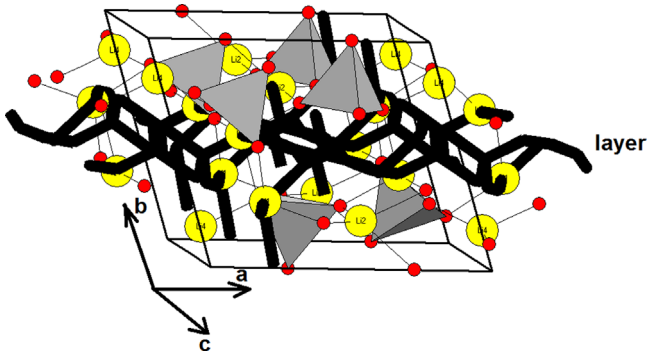

Fig. 9. Triclinic crystal structure of $Li_4P_2O_7$ at 300 K. Red balls represent oxygen atoms; black lines show Li^+ ion migration channels in the layers perpendicular to [010] direction. (For interpretation of the references to color in this figure legend, the reader is referred to the web version of this article.)

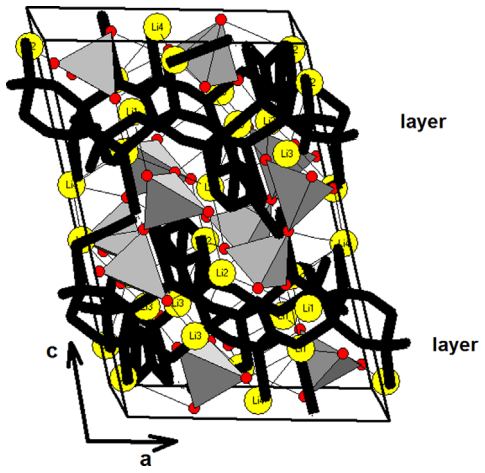

Fig. 10. Monoclinic crystal structure of $Li_4P_2O_7$ at 950 K. Red balls represent oxygen atoms; black lines show Li^+ ion migration channels in the layers perpendicular to [001] direction. (For interpretation of the references to color in this figure legend, the reader is referred to the web version of this article.)

to the [010] direction (Fig. 9). Therefore, the conductivity is anisotropic.

After phase transition at $T > 900$ K the monoclinic cell contains 43 significant voids, part of which is occupied by lithium ions. Such an increase of significant voids number occurs due to the doubling of the cell volume. Again, all significant voids and Li1, Li2, Li3 and Li4 positions are connected by significant channels. As in the case of triclinic form, the conductivity in monoclinic $Li_4P_2O_7$ is three-dimensional but most of the channels are located in the layers normal to [001] direction which is equivalent to [010] direction in triclinic cell (Fig. 10). Therefore, the conductivity in monoclinic form of $Li_4P_2O_7$ is anisotropic too. Significant ZA voids and Li1, Li2, Li3 and Li4 positions form an infinite chain of channels. The Li^+ ions migrate along these bent channels through the common faces of tetrahedra.

Fig. 11 shows an example temperature dependences of the radii of elementary channels through which a Li^+ ion has to pass to shift from Li1 to Li3 position via ZA1, ZA2 and ZA3 significant voids (top) and of the radii of elementary channels through which a Li^+ ion have to pass to shift from Li2 to Li1 position via ZA4 and ZA5 significant voids (bottom). As is well known, ion conductivity is limited by the minimum dimension of elementary channels (bottleneck) [33]. In our case, this is the channel connecting significant void ZA3 and Li3 position (top) or the channel connecting significant void ZA5 and Li1 position (bottom). One can see that the radii of these channels slightly exceed the critical value. With increasing temperature, the cross sections of the migration channels enlarge and at the phase transition a jump-like growth of bottleneck dimension is observed. This is one of the reasons for the jump-like conductivity increase at phase transition (Fig. 1). An additional mechanism that provides the increase of the ion conductivity arises from the correlation between the oscillations of the PO_4 tetrahedra that form the P_2O_7 groups and the mobility of the Li^+ ions.

4. Conclusion

The crystal structure of $Li_4P_2O_7$ has been refined by Rietveld technique using high temperature neutron diffraction over a wide temperature range. The analysis of crystal structure confirms a triclinic crystal system, space group *P*-1 (No. 2) for the low temperature form of $Li_4P_2O_7$. The crystal structure of $Li_4P_2O_7$ consists of heavily distorted LiO_4 tetrahedra and PO_4 tetrahedra which are connected by a common oxygen atom into P_2O_7 groups. Some of the LiO_4 tetrahedra are connected with each other and with P_2O_7 groups by common edges or vertices. A high temperature neutron diffraction study has shown an essential anisotropy of triclinic lattice expansion up to 900 K. Above this temperature

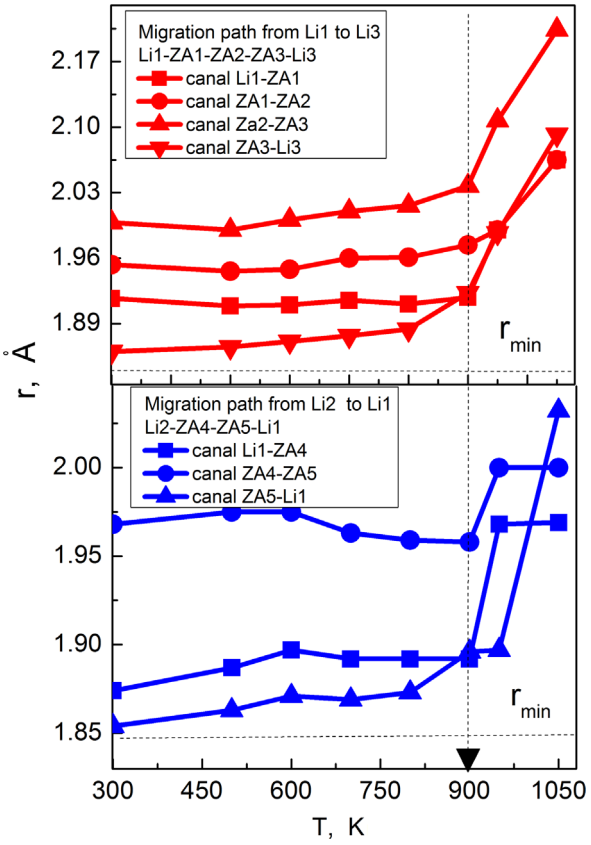

Fig. 11. Temperature dependences of radii of elementary channels between Li3 and Li1(top), Li2 and Li1(bottom) and significant voids ZA in the triclinic and monoclinic $Li_4P_2O_7$ phases.

the phase transition into monoclinic lattice takes place. The phase transition is accompanied by a jump-like increase of the ion conductivity. Similar behavior is shown by atom coordinates, thermal factors, etc., although the normalized lattice volume steadily increases. The analysis of the migration paths using the program package TOPOS shows that the cross section of migration channels increases with increasing temperature and undergoes a jump-like rise at the phase transition point. So, there exists a correlation between the ion conductivity of $Li_4P_2O_7$ and cross section of the migration channels. The diffuse scattering observed on the neutron diffraction patterns above the phase transition point shows that there is an additional mechanism that provides an increase of the ion conductivity due to the correlation between oscillations of the PO_4 tetrahedra that form the P_2O_7 groups and the mobility of the Li^+ ions.

Acknowledgments

This work was supported by Russian Foundation for Basic Research (grant No. 03-11-00663) and program of fundamental research of the Physics Division of RAS “Physics of new materials and structures” (No 12-T-2-1006). V.A.B. is grateful to the Russian government for support (Grant 14.B25.31.0005).

Appendix A. Supporting information

Supplementary data associated with this article can be found in the online version at http://dx.doi.org/10.1016/j.jssc.2013.12.015.

References

[1] M. Avdeev, V.B. Nalbandyan, I.L. Shukaev, in: V.V. Kharton (Ed.), Solid State Electrochemistry: Fundamentals, Methodology and Applications, Wiley-VCH, Weinheim, 2009, pp. 227–278.
[2] A.R. West, in: P.G. Bruce (Ed.), Solid State Electrochemistry, Cambridge University Press, Cambridge, 1995, pp. 7–43.
[3] E.I. Burmakin, G. Sh.Shekhtman, E.R. Aparina, E.S. Korovenkova, Russ. J. Electrochem. 28 (1992) 1240–1242.
[4] G. Sh.Shekhtman, E.I. Burmakin, E.S. Korovenkova, Russ. J. Electrochem. 33 (1997) 552–556.
[5] O.V. Yakubovich, O.K. Melnikov, Kristallografiya 39 (1994) 815–820.
[6] A. Daidouh, M.L. Veiga, C. Pico, M. Martinez-Ripoll, Acta Cryst. C53 (1997) 167–169.
[7] N.A.V. Holzwarth, N.D. Lepley, A.Du Yaojun, J. Power Sources 196 (2011) 6870–6876.
[8] L.N. Ji, J.B. Li, Y.Q. Chen, J. Luo, J.K. Liang, G.H. Rao, J. Alloys. Compd. 486 (2009) 352–356.
[9] D. Mazza, Mater. Lett. 7 (1988) 205–207.
[10] H. Hiooma, K. Hayashi, Mater. Res. Bull. 23 (1988) 1399–1407.
[11] J. Isasi, M.L. Veiga, C. Jerez, C. Pico, J. Less-Common Met. 167 (1991) 381–385.
[12] J. Isasi, M.L. Veiga, R. Saez-Pushe, C. Jerez, C. Pico, J. Alloys Compd. 177 (1991) 251–257.
[13] V. Thangadurai, S. Adams, W. Weppner, Chem. Mater. 16 (2004) 2998–3006.
[14] V.A. Blatov, IUCr CompComm Newslett. 7 (2006) 4.
[15] V.I. Voronin, M.G. Surkova, G. Sh.Shekhtman, N.A. Anurova, V.A. Blatov, Inorg. Mater. 46 (2010) 1234–1240.
[16] P. Fischer, G. Frey, M. Koch, M. Konnecke, V. Pomjakushin, G. Schefer, R. Thut, N. Schlumpf, R. Burge, U. Greuter, S. Bondt, S. Berruyer, Physica B276-278 (2000) 146–147.
[17] J. Rodriguez-Carvajal, Physica B192 (1993) 55–69.
[18] N.A. Anurova, V.A. Blatov, Acta Cryst. B65 (2009) 426–434.
[19] N.A. Anurova, V.A. Blatov, G.D. Ilyushin, O.A. Blatova, A.K. Ivanov-Schits, L.N. Dem'yanets, Solid State Ionics 179 (2008) 2248–2254.
[20] T.-Y. Tien, F.A. Hummel, J. Amer. Ceram. Soc. 44 (1961) 206–208.
[21] I.D. Brown, D. Altermatt, Acta Cryst. B41 (1985) 244.
[22] R.D. Shannon, Acta Cryst. A32 (1976) 751–767.
[23] V.I. Voronin, G. Sh.Shekhtman, V.A. Blatov, Acta Cryst. B68 (2012) 356–363.
[24] V.I. Voronin, V.A. Blatov, G. Sh.Shekhtman, Phys. Solid State 55 (2013) 1050–1056.
[25] D. Sheptyakov, N.Z. Ali, M. Jansen, J. Phys.: Condens. Matter 22 (2010) 426001.
[26] I.P. Swainson, V.T. Dove, J.Phys.: Condens. Mater. 7 (1995) 1771.
[27] A. Lunden, Solid State Commun. 85 (1988) 1237–1240.
[28] P. Zetterstrom, R.L. McGreevy, A. Mellergard, J. Eriksen, Appl. Phys. A74 (2002) 995–997.
[29] T. Sakuma, J. Tomas, J. Phys. Soc. Jpn. 62 (1993) 3127–3134.
[30] L. Nilsson, J. Thomas, B.C. Tofield, J. Phys. C13 (1980) 6441–6445.
[31] M. Arai, T. Shimoyama, T. Sakuma, H. Takahashi, Y. Ishii, Solid State Ionics 176 (2005) 2477–2480.
[32] T. Sakuma, T. Shimoyama, K. Basar, Xianglian, M. Arai, Y. Ishii, Solid State Ionics 176 (2005) 2689–2693.
[33] H.Y.-P. Hong, Mat. Res. Bull. 11 (1976) 173.